ACKNOWLEDGMENT

The authors would like to thank Dr. K. A. Rauschenbach for helpful technical suggestions.

REFERENCES

[1] S. A. Maas, *Nonlinear Microwave Circuits*. Norwood, MA: Artech House, 1988, pp. 283–319.
[2] C. Nguyen, "A 35% bandwidth Q-to-W-band frequency doubler," *Microwave J.*, pp. 232–235, Sept. 1987.
[3] J. W. Archer and M. T. Faber, "High-output, single- and dual-diode, millimeter-wave frequency doublers," *IEEE Trans. Microwave Theory Tech.*, vol. MTT-33, pp. 533–538, June 1985.
[4] P. Penfield, Jr. and R. P. Rafuse, *Varactor Applications*. Cambridge, MA: M.I.T. Press, 1962.
[5] K. Benson and M. A. Frerking, "Theoretical efficiency for triplers using nonideal varistor diodes at submillimeter wavelengths," *IEEE Trans. Microwave Theory Tech.*, vol. MTT-33, pp. 1367-1374, Dec. 1985.
[6] M. T. Faber, J. W. Archer, and R. J. Mattauch, "A frequency doubler with 35% efficiency at W band," *Microwave J.*, vol. 28, pp. 145–152, July 1985.
[7] M. V. Schneider and T. G. Phillips, "Millimeter-wave frequency multiplier," *Int. J. Infrared and Millimeter Waves*, vol. 2, pp. 15–22, 1981.
[8] M. V. Schneider and W. W. Snell, "A scaled hybrid frequency multiplier from 10 to 30 GHz," *Bell Syst. Tech. J.*, vol. 50, pp. 1933–1942, 1971.
[9] M. V. Schneider and W. W. Snell, "Hybrid integrated frequency multiplier from 10 to 30 GHz," *Proc. IEEE*, vol. 58, pp. 1402–1404, 1970.
[10] C. H. Page, "Harmonic generation with ideal rectifiers," *Proc. IRE*, vol. 46, pp. 1738–1740, Oct. 1956.
[11] C. H. Page, "Frequency conversion with positive nonlinear resistors," *J. Res. Nat. Bur. Stand.*, vol. 56, pp. 179–190, Apr. 1956.
[12] W. M. Van Loock, "Optimum frequency multiplication with resistive diodes," *Electron. Lett.*, vol. 10, pp. 158–159, May 2, 1974.
[13] P. Proksch, "Energetische Beziehungen für Bandbegrenzte Signale in Nichtinearen Wirkwidersanden," *Arch. Elek. Übertragung*, vol. 35, pp. 222–224, May 1981.
[14] D. Leenov and A. Uhlir, "Generation of harmonics and subharmonics at microwave frequencies with P-N junction diodes," *Proc. IRE*, vol. 46, pp. 1724–1729, Oct. 1959.
[15] J. M. Manely and H. E. Rowe, "Some general properties of nonlinear elements," *Proc. IRE*, vol. 44, pp. 904–913, July 1956.
[16] A. Sanchez, C. F. Davis, K. C. Liu, and A. Javan, "The MOM tunneling diode: Theoretical estimate of its performance at microwave and infrared frequencies," *J. Appl. Phys.*, vol. 49, no. 10, pp. 5270–5277, Oct. 1978.
[17] W. H. Press, B. P. Flannery, S. A. Teukolsky, and W. T. Vetterling, *Numerical Recipes: The Art of Scientific Computing*. New York: Cambridge University Press, 1986, pp. 254–259.
[18] J. W. Archer, "Millimeter wavelength frequency multipliers," *IEEE Trans. Microwave Theory Tech.*, vol. MTT-29, pp. 552–557, June 1981.
[19] N. R. Erickson, "A high efficiency frequency tripler for 230 GHz," in *Proc. 12th European Microwave Conf.*, Sept. 1982, pp. 288–298.
[20] J. W. Archer, "An efficient 200–290-GHz frequency tripler incorporation in a novel stripline structure," *IEEE Trans. Microwave Theory Tech.*, vol. MTT-32, pp. 416–420, Apr. 1984.
[21] K. Rauschenbach, "The self-aligned opposed gate–source transistor and the distributed thin film harmonic generator," Ph.D. thesis, Cornell University, 1988.
[22] K. C. Lee, J. Silcox, and C. A. Lee, "Schottky barrier diode on a submicron-thick silicon membrane using a dual surface fabrication technique," *J. Appl. Phys.*, vol. 60, no. 11, 1 Dec. 1986.
[23] K. Rauschenbach and C. A. Lee, "High-resolution resonant refractive index lithography," *J. Appl. Phys.*, vol. 66, no. 9, pp. 4481–4488, Nov. 1989.

Scattering Effects in the Dielectric Slab Waveguide Caused by Electrically Dissipative or Active Regions

Thomas G. Livernois, Dennis P. Nyquist, and Michael J. Cloud

***Abstract*—A polarization electric field integral equation (EFIE) is used to model conducting discontinuities in the dielectric slab waveguide. A complex refractive index accounts rigorously for effects of conduction current in the discontinuity region. Both dissipative and active cases are treated; power balance, based on Poynting's theorem, is used to determine the fractional radiated power in each case. The method of moments is invoked to solve the integral equation. The accuracy of the analysis method is confirmed through comparison of results for the air gap case with those of other recently published methods. Numerical results illustrate application to a typical GaAs ternary system.**

I. INTRODUCTION

Open dielectric waveguide components have become increasingly important research topics. These structures are involved in many crucial aspects of high-frequency integrated circuits. Waveguide discontinuities resulting from these components often give rise to problems in performance [1]; therefore, precise knowledge of discontinuity field behavior plays an important role in component and system design. Several approaches have been used for the analysis of open-boundary waveguide problems, including perturbation methods [2], spectral iterative techniques [3], and finite- and boundary-element methods [4]. A brief literature review may also be found in [4].

This paper treats phenomena associated with scattering from electrically dissipative or active slice discontinuities in the dielectric slab. The apparent absence of published work in this area seems to indicate that the effects of conduction currents within dielectric waveguide discontinuities have not been rigorously studied.

The present work exploits the polarization electric field integral equation (EFIE) formulation described and developed in [5]. The polarization EFIE is solved by the method of moments (MoM), leading to relevant discrete-mode scattering coefficients, and fractional powers (with respect to incident power) scattered, radiated, and dissipated/supplied (in the passive/active case). This method has several advantages over other existing approaches, viz., (1) it is conceptually exact, and (2) it is believed to be computationally less cumbersome than finite-element and related methods.

II. THEORY

Fig. 1 shows the configuration of the discontinuity region along an open-boundary dielectric slab waveguide. The refractive index profile of a uniform, unperturbed surface waveguide is described by n_g, while index n_s characterizes the uniform

Manuscript received January 2, 1990; revised October 23, 1990. This work was supported in part by the National Science Foundation under Grant ECS-86-11958.

T. G. Livernois is with the Department of Electrical Engineering and Computer Science, University of Michigan, Ann Arbor, MI 48109.

D. P. Nyquist is with the Department of Electrical Engineering, Michigan State University, E. Lansing, MI 48824.

M. J. Cloud is with the School of Engineering, Lawrence Technological University, Southfield, MI 48075.

IEEE Log Number 9042340.

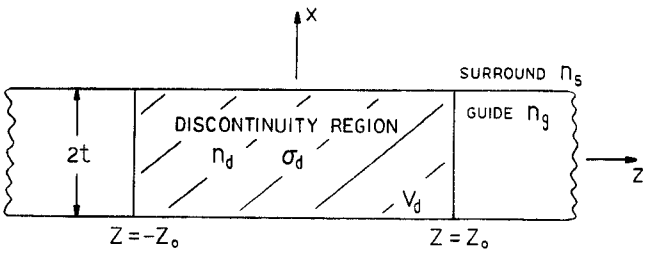

Fig. 1. Geometry of the problem.

surround medium. Surface waves incident upon the discontinuity are scattered in a manner dependent upon these indices and the physical geometry present. The waveguide system parameters are chosen so that only the dominant TE surface-wave mode exists.

The incident surface-wave mode, maintained by a remote impressed source current $\vec{J}^e$, illuminates the discontinuity. The integral equation describing this system originates with the identification of an equivalent polarization distribution $\vec{P}_{eq} = \epsilon_0 \delta n^2(r)\vec{E}$ and its associated polarization current $\vec{J}_{eq} = j\omega\vec{P}_{eq}$. Here $\delta n^2 = n_d^2 - n_g^2$ is the refractive index contrast, which is nonzero only in the discontinuity region. The total field within V_d is equal to the sum of the incident field $\vec{E}^i$ and the scattered field $\vec{E}^s$, where $\vec{E}^s$ is excited by $\vec{J}_{eq}$. Expressing $\vec{E}^s$ as the integral of the inner product of $\overleftrightarrow{G}$ and $\vec{J}_{eq}$ over that region where $\delta n^2 \neq 0$, we may write

$$\vec{E}(\vec{r}) - j\omega\epsilon_0 \delta n^2 \int_{V_d} \overleftrightarrow{G}(\vec{r}|\vec{r}') \cdot \vec{E}(\vec{r}')\, dv' = \vec{E}^i(\vec{r}) \quad \text{for all } \vec{r} \in V_d. \tag{1}$$

$\overleftrightarrow{G}$ is the electric Green's dyadic for the planar, layered environment and $\vec{E}^i(\vec{r}) = \hat{y}E_0 e_{y0}(x,y)\exp(-j\beta_0 z)$ at points $\vec{r} \in V_d$, where e_{y0} is the electric field profile of the principal TE mode and β_0 is its propagation constant. Solutions to the EFIE (1), for $\vec{E}$ excited in V_d, lead subsequently to the scattered (reflected, transmitted, and radiated) fields exterior to V_d.

Specializing (1) to the y-invariant geometry of Fig. 1 leads to the following 2-D scalar integral equation:

$$E_y(x,z) - j\omega\epsilon_0 \delta n^2 \int_{-z_0}^{z_0}\int_{-t}^{t} E_y(x',z') G_{yy}(x,z|x',z')\, dx'\, dz'$$
$$= E_0 e_{y0}(x)\exp(-j\beta_0 z) \quad \text{for all } |x| \leq t, \quad |z| \leq z_0 \tag{2}$$

where the electric Green's function

$$G_{yy}(x,z|x',z') = -e_{y0}(x)e_{y0}(x')\exp(-j\beta_0|z-z'|)$$
$$-\int_0^\infty e_y(x,\lambda)e_y(x',\lambda)\exp(-j\beta(\lambda)|z-z'|)\, d\lambda \tag{3}$$

with $e_y(x,\lambda)$ the appropriately normalized continuous spectrum field, is detailed in [5]–[7].

Nonvanishing discontinuity region conductivity is incorporated into a complex refractive index describing that region. This index is expressed as $n_d = n_r - jn_i$, where n_i is negative/positive for the active/passive case. The real and imaginary parts of n_d are related to the conductivity σ_d by the equation

$$n_i = \sigma_d Z_0 \lambda_0 / 4\pi n_r \tag{4}$$

where $Z_0 = (\mu_0/\epsilon_0)^{1/2}$ is the free-space intrinsic impedance, and λ_0 is the free-space operating wavelength.

A power balance requirement forms the basis for calculating power radiated from the discontinuity region. Incident surface-wave power P_{INC}, power P_{DISC} supplied/dissipated by the discontinuity, and the reflected, transmitted and radiated powers P_{REFL}, P_{TRAN}, and P_{RAD}, respectively, are related by

$$P_{INC} + P_{DISC} = P_{REFL} + P_{TRAN} + P_{RAD}$$
$$= |R_0|^2 P_{INC} + |T_0|^2 P_{INC} + P_{RAD}. \tag{5}$$

The power supplied/dissipated, by Poynting's theorem, is

$$P_{DISC} = -\frac{1}{2}\,\mathrm{Re}\left\{\int_{V_d} \vec{J}\cdot\vec{E}\, dv\right\} = -\frac{\sigma_d}{2}\int_{V_d} |\vec{E}|^2\, dv. \tag{6}$$

When $\sigma_d < 0$, then $P_{DISC} = P_{SUPP}$ is power supplied, while $P_{DISC} = -P_{DISS} < 0$ represents dissipated power when $\sigma_d > 0$. The power carried by the incident wave is

$$P_{INC} = (\beta/\omega\mu_0)\int_0^\infty |E_0 e_{y0}(x)|^2\, dx. \tag{7}$$

Reflection coefficient R_0 and transmission coefficient T_0 are defined as the ratios of the back- and forward-scattered principal-mode surface waves, respectively, to the incident wave at terminal planes located at the discontinuity extremities. Overlap-integral expressions for those principal mode scattering coefficients are given in [5].

In the following section we give numerical results for scattering coefficients and power quantities obtained for various cases of lossless, passive, and active discontinuity region parameters.

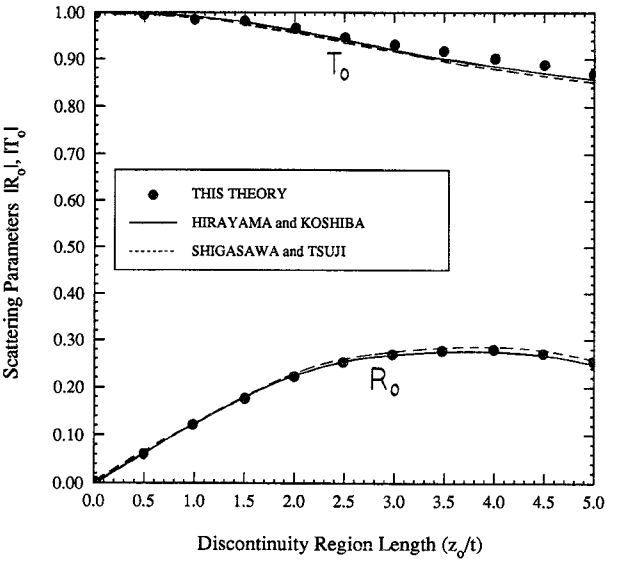

Fig. 2. Comparison of scattering coefficient magnitudes for air gap with data from other methods.

III. Results

The MoM numerical solution of (5) is implemented by using 2-D pulse expansion functions, in a rectangular partitioning of N_x by N_z segments in the x and z directions, respectively. Pulse functions are also used for testing (Galerkin's method). Convergence of the numerical solution is assessed by numerical experimentation with the partition mesh sizes through N_x and N_z.

Figs. 2 and 3 compare the EFIE's performance with two other methods [1], [4] for an air gap with $n_d = 1$. Here, scattering coefficients R_0 and T_0 are plotted versus normalized length of the discontinuity region. Note that these figures are data for the case having $n_g = 2.236$, $n_s = 1.0$, and $t/\lambda_0 = (10\pi)^{-1}$. Dominant TE mode scattering coefficients show excellent agreement for the magnitude of R_0 and a very good match for the magnitude of T_0 (with a maximum difference of 3%). Fig. 3 shows virtually exact agreement for the phases of R_0 and T_0.

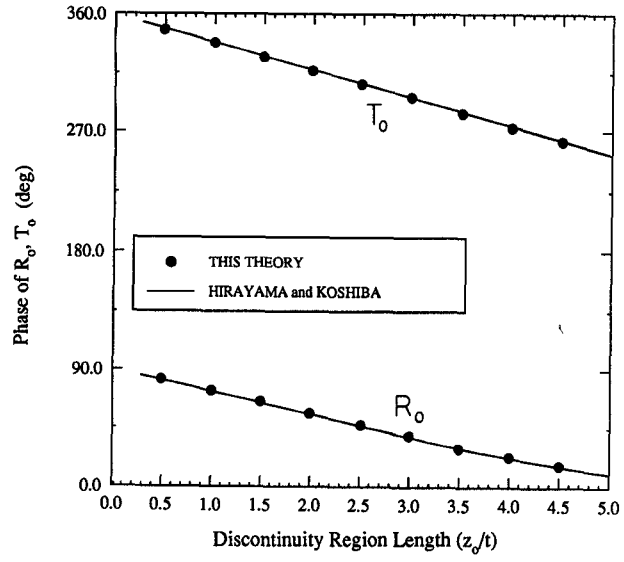

Fig. 3. Comparison of scattering coefficient phases for air gap with other data from other methods.

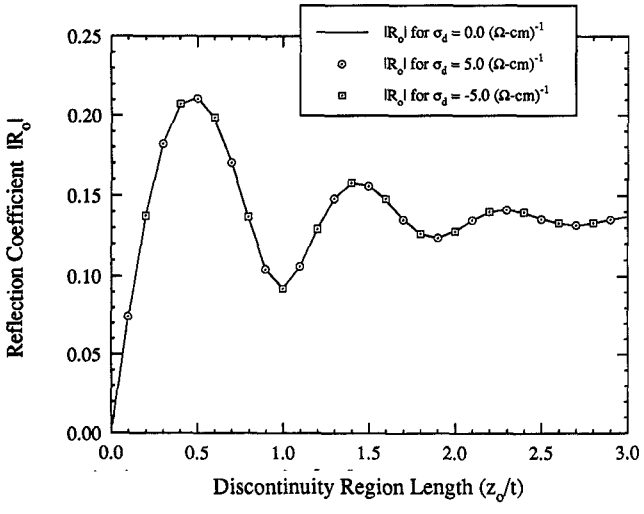

Fig. 4. Plot of reflection coefficient magnitude versus discontinuity region length for various values of conductivity.

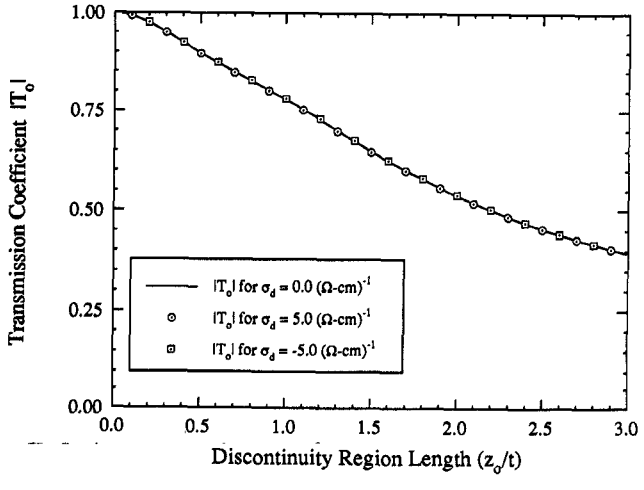

Fig. 5. Plot of transmission coefficient magnitude versus discontinuity region length for various values of conductivity.

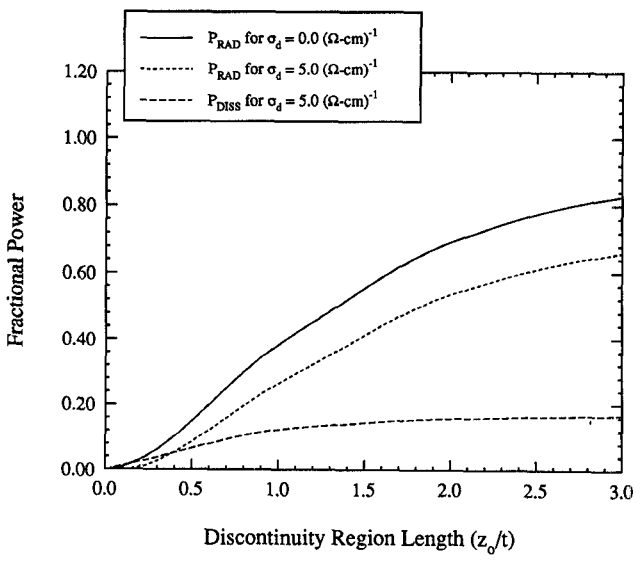

Fig. 6. Fractional power versus discontinuity region length for dissipative case.

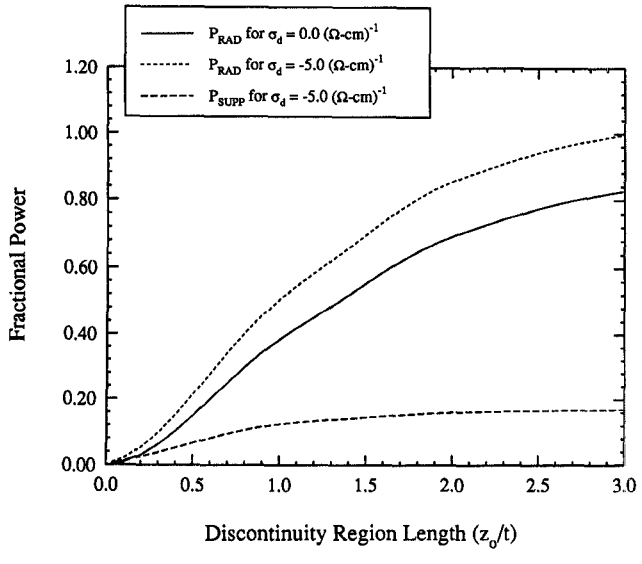

Fig. 7. Fractional power versus discontinuity region length for active case.

The remaining results have waveguide system parameters chosen to approximately model a GaAs ternary system having $n_g = 3.6$, $n_s = 3.3$, $t/\lambda_0 = 0.1$, $\lambda_0 = 0.87$ μm, and $\beta_0 t = 2.153$, where β_0 is the phase constant of the dominant TE mode. Figs. 4 and 5 exhibit the magnitudes of R_0 and T_0 versus discontinuity region length for $n_d = 2.5$ and for various values of discontinuity region conductivity. Scattering coefficients for the discrete mode are virtually identical for all three cases plotted here. Fig. 6 shows corresponding radiated and dissipated power values and compares these with the lossless case. Fig. 7 displays radiated and supplied power quantities versus discontinuity region length and compares these with P_{RAD} for the lossless case.

To help explain why the radiation field is primarily affected while the discrete field scattering coefficients are largely unchanged, we offer spatial intensity distribution plots of the electric field in the discontinuity in Figs. 8 through 11. Note that z_0/t is fixed at 1.0 for these cases, and since the fields have symmetry with x, only the field for $0 < x < t$ is depicted. Fig. 8 is the unperturbed case, displaying the expected transverse,

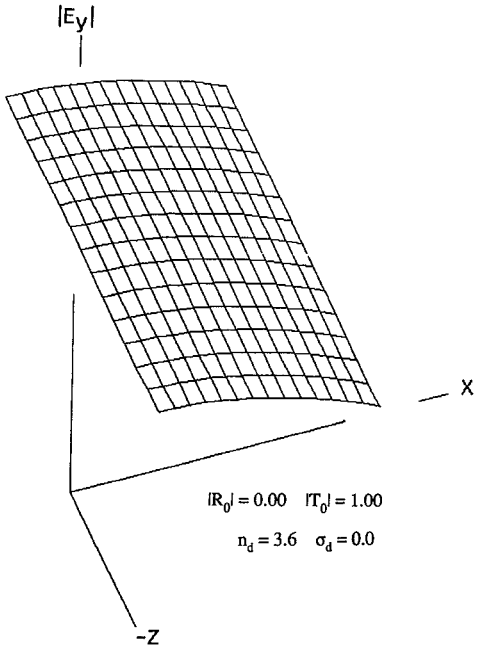

Fig. 8. Spatial variation of unperturbed waveguide mode.

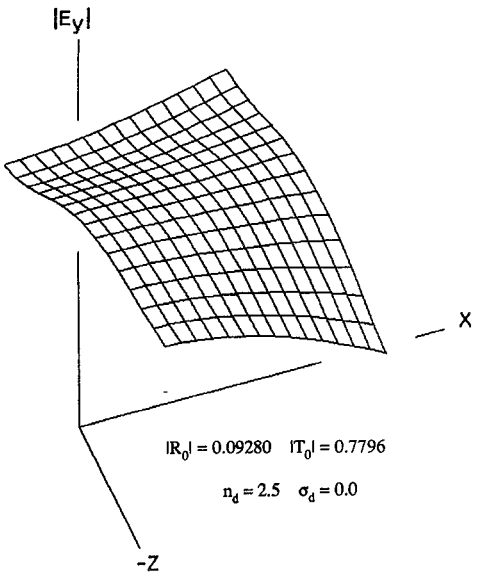

Fig. 9. Spatial variation of total discontinuity region field: lossless case.

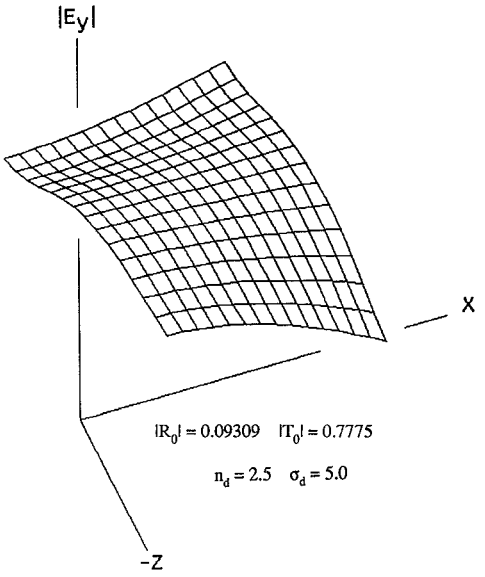

Fig. 10. Spatial variation of total discontinuity region field: dissipative case.

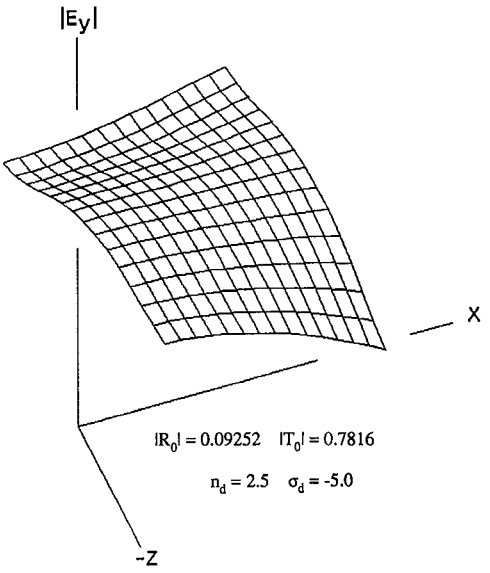

Fig. 11. Spatial variation of total discontinuity region field: active case.

slowly varying, weakly guided cosine distribution (i.e., the incident mode). For this figure $n_d = n_g = 3.6$. Figs. 9 through 11 have $n_d = 2.5$. Fig. 9 shows the total field in the zero-conductivity case; Fig. 10 has $\sigma_d = 5$; Fig. 11 represents the active case with $\sigma_d = -5$. It is clear that the field distribution within the discontinuity region is essentially the same for all three cases. The coefficients R_0 and T_0 are calculated using overlap integrals involving the incident modal field and the total field in the discontinuity; therefore, if the total field changes slightly, the discrete-mode scattering coefficients differ only slightly. In sharp contrast, Fig. 12 shows the field for $n_d = 5.5$ and $\sigma_d = 0$; this graph clearly illustrates the effect of discontinuity region field variation on R_0 and T_0.

IV. Discussion

This paper presents an analysis of scattering from electrically active or dissipative dielectric-slab waveguide discontinuities. This EFIE-based method is conceptually exact, and the accuracy of its numerical solution is verified by comparison with published air-gap discontinuity results. Other numerical results given correspond approximately to a uniform discontinuity region in a GaAs ternary system. Both passive and active conduction currents are considered in this analysis.

In a junction between two dielectric waveguides, it appears that radiation can be reduced by adding a dopant in the junction vicinity (see Fig. 6); in this case the discrete mode remains largely unaffected. It is hoped that future research will confirm this hypothesis. It should be mentioned that to obtain an amplified *discrete* mode in a region where the conductivity σ_d is representative of a realistic value for an internal laser gain [8]

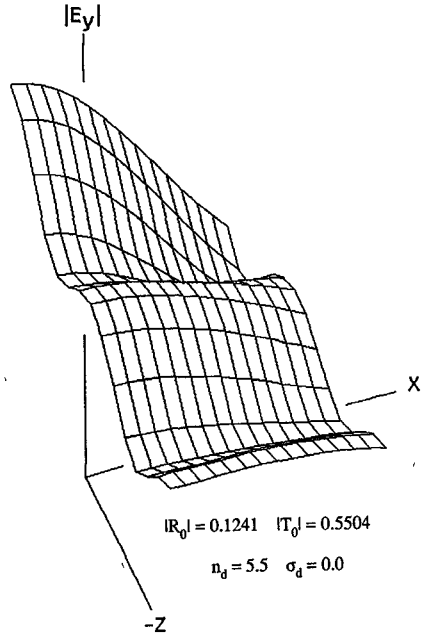

Fig. 12. Spatial variation of total discontinuity region field for large refractive index contrast.

one of the following becomes necessary: distributed feedback, a nonuniform gain profile according to the Bragg diffraction rule, or use of a Fabry–Perot resonator. Moreover, the gain region must be hundreds of wavelengths long, which is computationally prohibitive for the MoM at present.

Acknowledgment

The authors thank Dr. Herbert Winful of the University of Michigan Optical Sciences Laboratory and Dr. Glen Feak of the University of Michigan Center for High-Frequency Microelectronics for their helpful suggestions.

References

[1] H. Shigesawa and M. Tsuji, "A new equivalent network method for analyzing discontinuity properties of open dielectric waveguides," *IEEE Trans. Microwave Theory Tech.*, vol. 37, pp. 3–14, Jan. 1989.

[2] E. G. Rawson, "Analysis of scattering from fiber waveguides with irregular core surfaces," *Appl. Opt.*, vol. 13, no. 10, pp. 2370–2377, Oct. 1974.

[3] S. Ray and R. Mittra, "Numerical analysis of open waveguide discontinuities," *Radio Sci.*, vol. 19, no. 5, pp. 1289–1293, Sept.–Oct. 1984.

[4] K. Hirayama and M. Koshiba, "Analysis of discontinuities in an open dielectric slab waveguide by combination of finite and boundary elements," *IEEE Trans. Microwave Theory Tech.*, vol. 37, pp. 761–768, Apr. 1989.

[5] T. G. Livernois and D. P. Nyquist, "Integral-equation formulation for scattering by dielectric discontinuities along open-boundary dielectric waveguides," *J. Opt. Soc. Amer. A*, vol. 4, 1289–1295, 1987.

[6] D. P. Nyquist, D. R. Johnson, and S. V. Hsu, "Orthogonality and amplitude spectrum of radiation modes along open-boundary waveguides," *J. Opt. Soc. Amer.*, vol. 71, pp. 49–54, Jan. 1981.

[7] T. E. Rozzi, "Rigorous analysis of the step discontinuity in a planar dielectric waveguide," *IEEE Trans. Microwave Theory Tech.*, vol. MTT-26, pp. 738–746, Oct. 1978.

[8] B. S. Poh, "Refractive index to gain derivative ratio in GaAs/GaAlAs semiconductor injection lasers," *Proc. Inst. Elect. Eng.*, pt. I, vol. 131, pp. 163–169, Oct. 1984.

Toward a Unified Efficient Algorithm for Characterizing Planar Periodic Waveguides and Their Applications to MIC and MMIC Circuits

Ké Wu, Pierre Saguet, and André Coumes

Abstract—**An efficient new algorithm (modified three-dimensional spectral-domain solution with "modal spectrum") applied to a variety of planar waveguides with periodically loaded stubs is achieved. In this paper, slow-wave propagation characteristics and their mechanism of both symmetrically and asymmetrically loaded periodic structures with lossy dielectric layer such as finline and coplanar waveguides (CPW's) are investigated. Using two sets of familiar basis functions, the convergence behavior of the high-speed numerical computation is presented toward a unified efficient algorithm. Many important features such as passband and stopband phenomena related to cutoff and resonant frequencies are discussed in detail based on numerical results, which are compared with measured results obtained by transmission line experimental procedures**

I. Introduction

With increasing development of millimeter-wave transmission line media and monolithic integrated circuit technologies, there has been growing interest in the properties of hybrid (nonuniform) structures in the transverse section as well as the longitudinal section to realize a more compact package, easier serial implementation, and wider monomode operation. Many planar or quasi-planar waveguides such as finlines and suspended striplines have been suggested and investigated in the frequency range $10 \sim 150$ GHz. Little or rather limited information about the nonuniform longitudinal structures has been published, for example, information relating to periodically loaded lines.

On the other hand, coplanar waveguide (CPW) and finline MIS (metal–insulator–semiconductor) structures proposed and analyzed recently by several authors [1]–[5] in an attempt to realize the phase shifters, delay lines, and electronically variable filters make it possible to reduce significantly the component dimensions due to the slow-wave propagation with possible smaller losses. However, the question concerning an efficient slow-wave mode excitation and miniature interconnection of circuits will need to be addressed.

One way to obtain a slow wave is to guide the wave in a direction away from the desired axial direction and to use the axial components. It should be pointed out that a main mechanism of obtaining a slowing down (high $\epsilon_{\text{eff}} = (\lambda_{\text{air}}/\lambda_{\text{guide}})^2$) of propagation is to store the electric and magnetic energy separately in space whether it is transversal or longitudinal. Examples of such structures include the MIS, helix, meander interdig-

Manuscript received March 27, 1987; revised September 17, 1990.

K. Wu was with LEMO-ENSERG, 23 Avenue des Martyrs, BP 257, 38016 Grenoble, France. He is now with the Department of Electrical and Computer Engineering, University of Victoria, PO Box 3055, Victoria, B.C., Canada V8W 3P6.

P. Saguet and A. Coumes are with LEMO-ENSERG, 23 Avenue des Martyrs, BP 257, 38016 Grenoble, France.

IEEE Log Number 9042342.